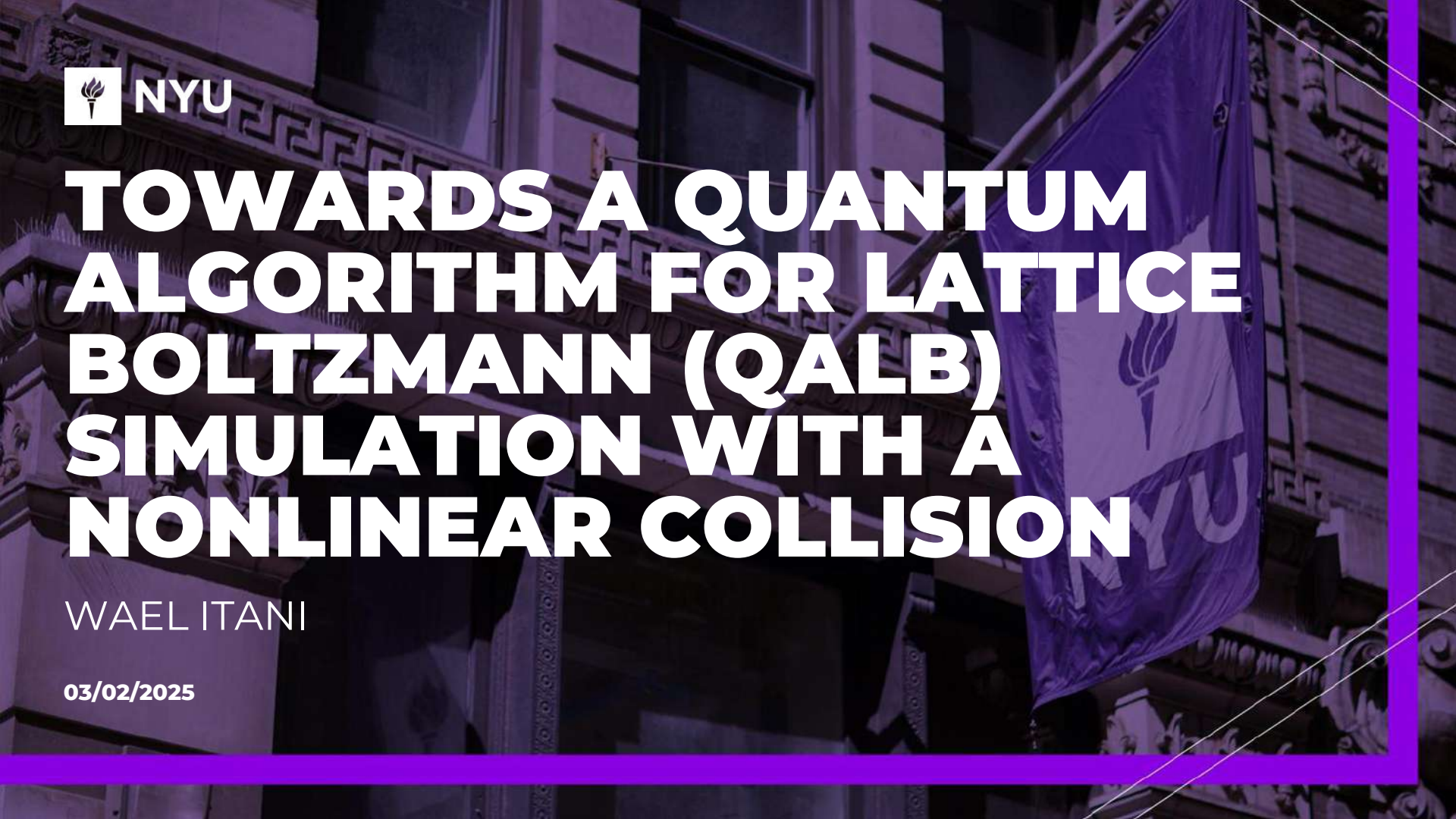

NYU

TOWARDS A QUANTUM ALGORITHM FOR LATTICE BOLTZMANN (QALB) SIMULATION WITH A NONLINEAR COLLISION

WAEL ITANI

03/02/2025

CONTENTS

NYU

PROLOGUE

00

The Market & Cost of CFD

NYU

CFD MARKET

$1 bln.

(7% CAGR 2020-2030

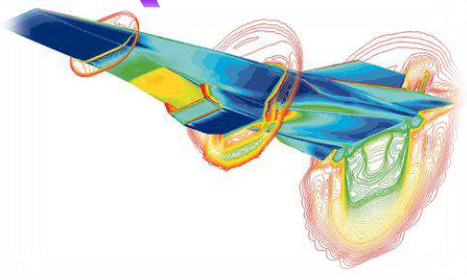

Visualization of CFD results for Mach 7 flight (NASA, 1997)

Minimally invasive cancer detection with microfluidic chip (University of Kansas, 2019)

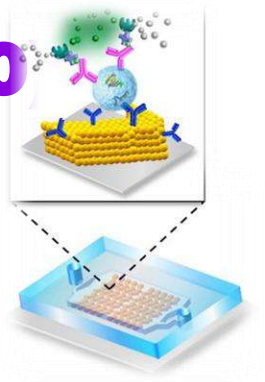

NYU

COMPUTATIONAL COST

DNS (Scale-resolved) ~ Re^{3}

LES (Filtered scales) ~ $Re^{1.3\sim2.5}$

Re_c	N_{dof}	N_{iter}	FLOP	PFLOP/s
1e6	9.0e9	4.6e7	5.2e20	6
1e7	8.5e10	1.5e8	1.6e22	180
1e8	7.5e11	4.6e8	4.3e23	5,000

Estimates for wall-resolved LES as a function of the Reynolds number (CFD Vision 2030, NASA, 2014)

$Re > \sim 10^{5}$

(Teapeat, 2012)

BOLTZMANN'S REACH

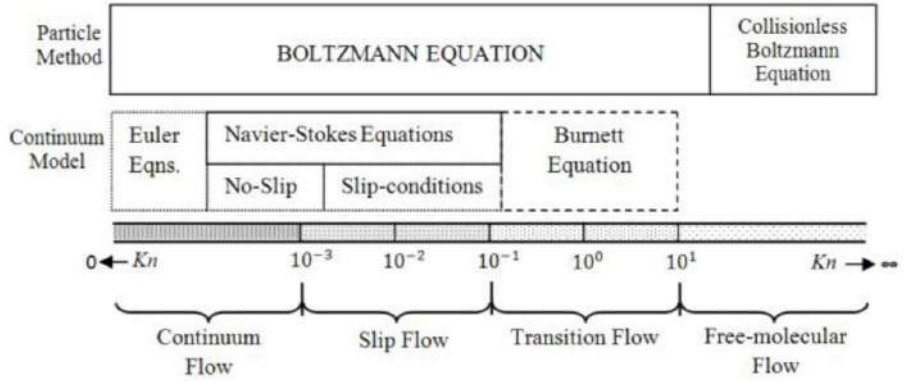

Applicability of a range of fluid models based on the Knudsen number (Ayub et al., 2011)

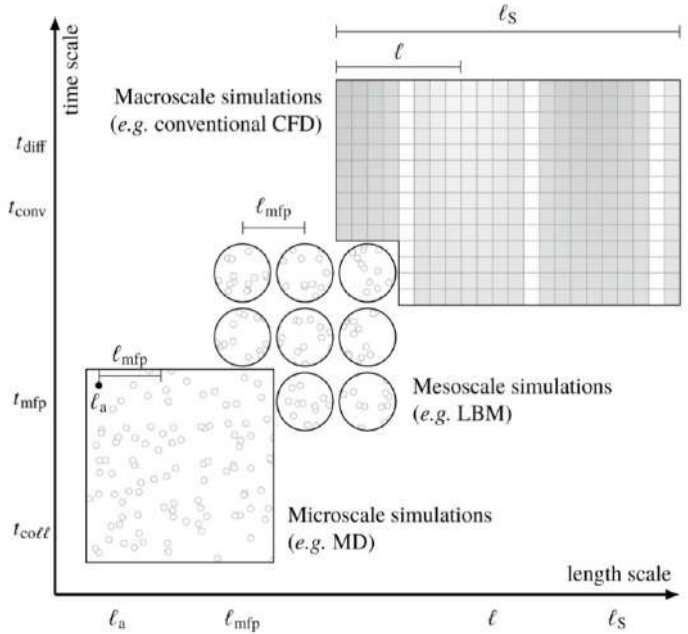

Hierarchy of length and time scales in typical fluid dynamics problems (Chaves-Modena, 2019)

NYU

BEYOND BOLTZMANN

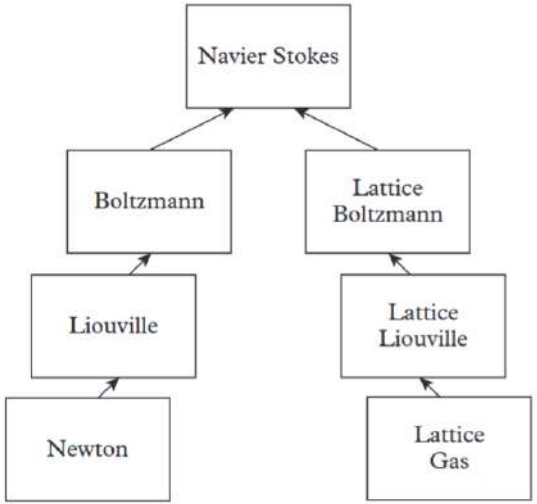

(Succi, 2018)

Binary collisions

Boltzmann $\xrightarrow{f = f^{(0)} + \epsilon f^{(1)} + \epsilon^2 f^{(2)} + \cdots}$ Navier-Stokes

$f^{(1)} \uparrow f^{(l)}$

BBGKY $\xleftarrow{f^{(l)} \leftarrow f^{(N)}}$ Liouville

LIOUVILLE & ITS MARGINALIZATION

$$\partial_t f^{(N)} + \Sigma_{i=1}^{N} (\vec{v}_i \cdot \partial_{\vec{x}_i} f^{(N)} + \Sigma_{j \neq i}^{l} \frac{1}{m} \vec{F}_{i,j} \cdot (\partial_{\vec{v}_i} f^{(N)} - \partial_{\vec{v}_j} f^{(N)})) = 0 \qquad (3.3)$$

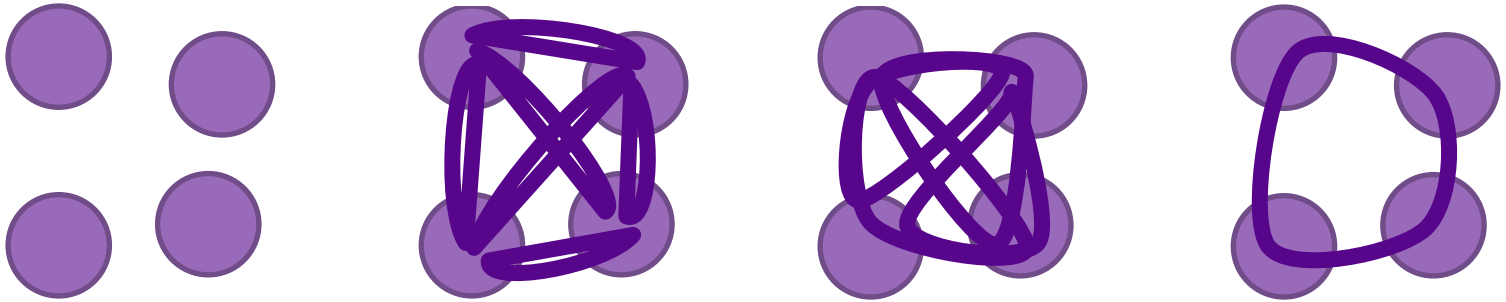

$$\partial_t f^{(l)} + \Sigma_{i=1}^{l} (\vec{v}_i \cdot \partial_{\vec{x}_i} f^{(l)} + \Sigma_{j \neq i}^{l} \frac{1}{m} \hat{F}_{i,j} f^{(l)}) = \Sigma_{i=1}^{l} \int \vec{F}_{i,l+1} \cdot \partial_{\vec{v}_i} f^{(l+1)} d\vec{\zeta}_{l+1} \qquad (3.1)$$

METHODS

12

The Lattice Boltzmann Method (LBM)

NYU

LATTICE BOLTZMANN

$$\frac{df}{dt} = \frac{\partial f}{\partial t} + \vec{v} \cdot \vec{\nabla} f = \Omega \qquad (1.1)$$

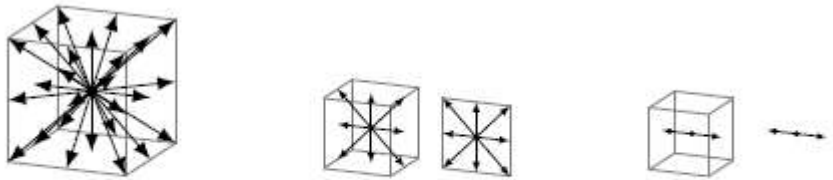

(a) D3Q27 (b) D2Q9 (c) D1Q3

Figure 1.1: Different lattice configurations in three, two and one dimensions

$$\frac{1}{\Delta t}\left(f_i(\vec{x} + \vec{c}_i \Delta t, t + \Delta t) - f_i(\vec{x}, t)\right) = -\frac{1}{\tau}\left(f_i(\vec{x}, t) - f_i^{eq}(\vec{x}, t)\right) \qquad (1.2)$$

$$f_i^{eq} = w_i \rho \left(1 + \frac{\vec{e}_i \cdot \vec{u}}{c^2} + \frac{(\vec{e}_i \cdot \vec{u})^2}{2c^4} - \frac{\vec{u}^2}{2c^2}\right) \qquad (3.105)$$

LATTICE BOLTZMANN

Collision (Local, nonlinear, dissipative)

$$f_i(\vec{x}, t + \Delta t) = f_i(\vec{x}, t) - \frac{\Delta t}{\tau}(f_i(\vec{x}, t) - f_i^{eq}(\vec{x}, t))$$

(a) Pre-Collision (b) Post-Collision (c) Streaming

$$f_i(\vec{x}, t + \Delta t) \rightarrow f_i(\vec{x} + \vec{c}_i \Delta t, t + \Delta t)$$

Streaming (Nonlocal, linear, unitary)

COLLISION DATASET GENERATION

Quantity	Minimum Value	Maximum Value
u	0	0.1
ρ	0.95	1.05
σ	10^{-15}	5×10^{-4}
τ	1	1

Table 5.1: Summary of the prescribed quantities describing the distributions of random variables used in generating the dataset

$f_i^{eq}(\rho, \vec{u})$ $\vec{u} = u_0(\cos(\theta), \sin(\theta))^T$

Random discrete density perturbations $f_i^{'neq}$ are sampled from a normal distribution

$f_i^{pre} = f_i^{eq} + f_i^{neq}$ $f_i^{neq} = f_i^{'neq} - \frac{1}{9}\rho' - \frac{1}{6}\vec{e}_i \cdot \rho'\vec{u}'$

METHODS

Carleman Linearization (CL)

13

NYU

CARLEMAN LINEARIZATION

$$\vec{V} = \begin{pmatrix} \vec{V}^{(1)} \\ \vec{V}^{(2)} \end{pmatrix} = \begin{pmatrix} f_1 \\ f_2 \\ f_3 \\ f_1^2 \\ f_1 f_2 \\ f_2^2 \\ f_2 f_3 \\ f_3^2 \\ f_3 f_1 \end{pmatrix} = \begin{pmatrix} V_1 \\ V_2 \\ V_3 \\ V_4 \\ V_5 \\ V_6 \\ V_7 \\ V_8 \\ V_9 \end{pmatrix} \tag{3.61}$$

$$\frac{\partial f_i(t)}{\partial t} = \Omega_i(\vec{f}(t)) \tag{3.62}$$

Carleman variables vector:

$$\frac{\partial \vec{V}(t)}{\partial t} = C\vec{V}(t) \tag{3.63}$$

where the Carleman linearization matrix C is obtained by deriving the following system of equations:

$$\frac{\partial V_n}{\partial t} = \Sigma_{i=1}^{Q} \frac{\partial V_n(t)}{\partial f_i} \Omega_i(f(t)) \tag{3.64}$$

METHODS

Quantum Computing (QC)

15

NYU

QUANTUM COMPUTING

- **Statevector**

$|0\rangle = \begin{pmatrix}1\\0\end{pmatrix}$ and $|1\rangle = \begin{pmatrix}0\\1\end{pmatrix}$

$$|\psi\rangle = \frac{C_0|0\rangle + C_1|1\rangle}{\sqrt{|C_0|^2 + |C_1|^2}}$$

$|\psi\rangle = C_0|0\rangle + C_1|1\rangle$
$|C_0|^2 + |C_1|^2 = 1$
$|\psi\rangle = e^{i\theta}|\psi\rangle$

- **Evolution**
  - **Unitary**

$\|\psi'\| = \|\psi\| = 1$
$|\psi'\rangle = \hat{U}|\psi\rangle, \hat{U}^\dagger\hat{U} = \hat{I}$

$i\hbar\partial_t|\psi\rangle = \hat{H}|\psi\rangle, \hat{H} = \left(\hat{H}^*\right)^T$

  - **Non-Unitary**

$|\psi\rangle \longrightarrow |0\rangle \; OR \; |1\rangle$

$P(|0,1\rangle) = |C_{0,1}|^2$

- **Advantages**
  - **Computational Space**

$|\psi_{\#qubits=2}\rangle \rightarrow |00_2 = 0_{10}\rangle$
$OR\ |01 = 1_{10}\rangle$
$OR|10 = 2_{10}\rangle$
$OR\ |11 = 3_{10}\rangle$

  - **Parallelism**

$U|\psi\rangle = C_0U|0\rangle + C_1U|1\rangle$

NYU

METHODS

Existing Literature for the LBM with QC

16

NYU

BITSHIFT STREAMING

$$|\psi(t)\rangle = \frac{1}{\sqrt{G}} \sum_{\vec{x} \in G} \sum_{i=1}^{Q} |f_i(\vec{x}, t)\rangle \, |\vec{e}_i\rangle \, |\vec{x}\rangle$$

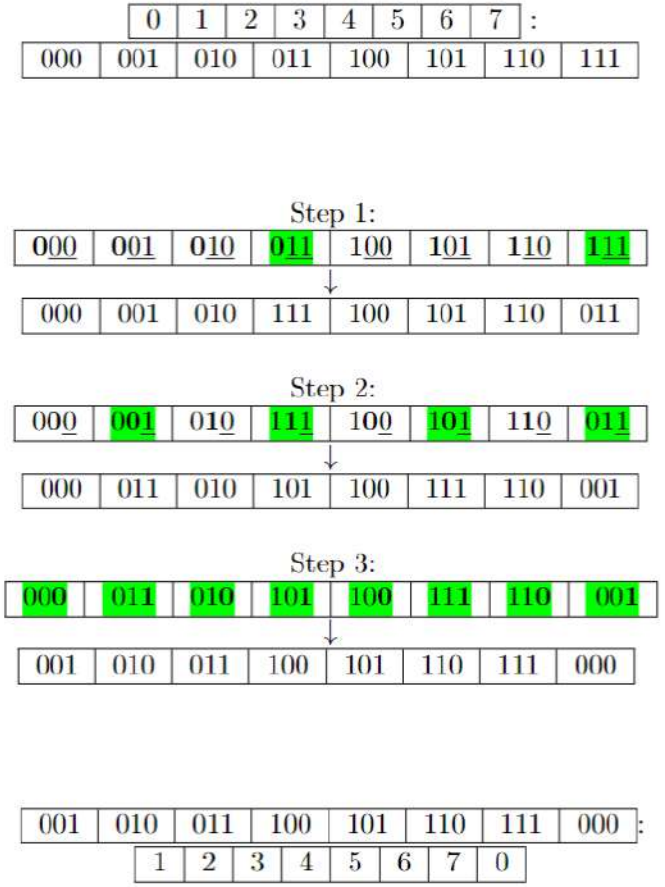

A visualization of the index-shuffling streaming procedure with periodic boundaries for 2^3 = 8 sites with a single variable. Contents of the cell refer to the corresponding index position. Green cells refer to the case where the condition of the control has been met and the digit being acted upon would change. Digits in binary representation being acted on by a controlled NOT gate (targets) are written in boldface whereas those controlling (controls) are underlined. The number of steps (3) is logarithmic in the number of sites (8)

NYU

QUANTUM SIMULATION

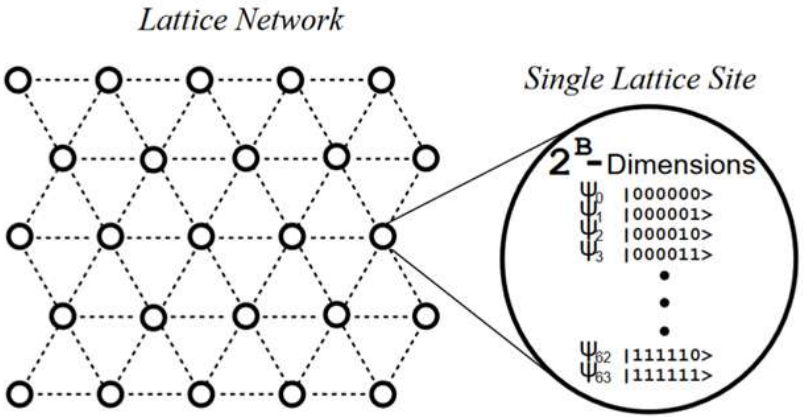

Quantum Lattice Gas

Depiction of the arrangement of 6-qubit quantum computers, each coupled to its neighbors to implement the quantum lattice gas algorithm (Yepez, 1999)

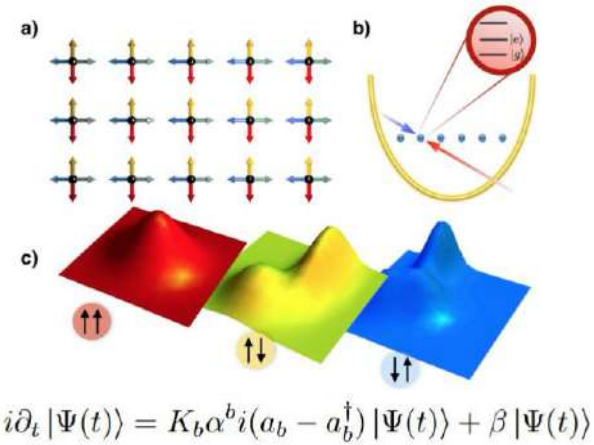

Dirac Analogy

The analogy between the Dirac and Boltzmann equations is employed to implement a lattice scheme with a dissipative linear collision (Mezzacapo et al., 2015).

NYU

PREVIOUS ATTEMPTS OF LBM WITH QC

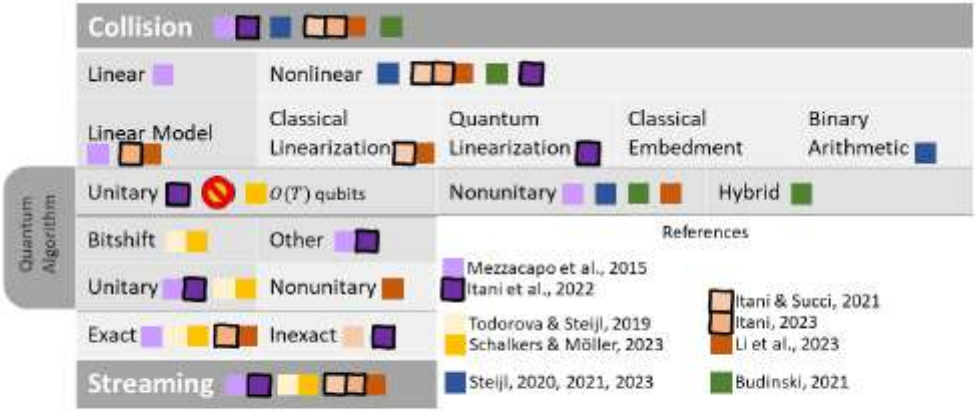

Figure 1.3: Main lines of research for the approaches on a quantum algorithm for the lattice Boltzmann method.

METHODS

Quantum Linear Embedding (QLE)

15

NYU

QUANTUM LINEAR EMBEDDING

$$u \to \hat{u}. \tag{4.2}$$

$$\begin{aligned} |x\rangle |y\rangle |z\rangle &= (\Sigma_{i,j,k=0}^{O_c} x^i |i\rangle)(\Sigma_{j=0}^{O_c} y^j |j\rangle)(\Sigma_{k=0}^{O_c} z^k |k\rangle) \\ &= \Sigma_{i,j,k=0}^{O_c} x^i y^j z^k |i\rangle |j\rangle |k\rangle , \end{aligned} \tag{4.1}$$

$$\frac{1}{\sqrt{0!}} = 1, \frac{u}{\sqrt{1!}} = u, \frac{u^2}{\sqrt{2!}}, \frac{u^3}{\sqrt{3!}}. \tag{4.9}$$

This encoding is known in quantum jargon, up to a normalization factor, as a coherent state

$$|\alpha\rangle = \Sigma_{n=0}^{\infty} \frac{\alpha^n}{\sqrt{n!}} |n\rangle , \tag{4.10}$$

$$\hat{a}|n\rangle = \sqrt{n}\,|n-1\rangle . \tag{4.12}$$

$$\hat{a} = \begin{pmatrix} 0 & 0 & 0 & 0 & \dots & 0 & \dots \\ \sqrt{1} & 0 & 0 & 0 & \dots & 0 & \dots \\ 0 & \sqrt{2} & 0 & 0 & \dots & 0 & \dots \\ 0 & 0 & \sqrt{3} & 0 & \dots & 0 & \dots \\ \vdots & \vdots & \vdots & \ddots & \ddots & \dots & \dots \\ 0 & 0 & 0 & \dots & \sqrt{n} & 0 & \dots \\ \vdots & \vdots & \vdots & \vdots & \vdots & \ddots & \ddots \end{pmatrix}$$

NYU

EVOLUTION UNDER QUANTUM LINEAR EMBEDDING

$$\hat{q} = \frac{1}{\sqrt{2}}(\hat{a} + \hat{a}^\dagger) \tag{4.16}$$

$$\hat{p} = -\frac{i}{\sqrt{2}}(\hat{a} - \hat{a}^\dagger). \tag{4.17}$$

$$|f\rangle = |q = f\rangle \tag{4.25}$$

$$\hat{q}|f\rangle = f|f\rangle \tag{4.26}$$

$$|f\rangle = e^{-i\hat{p}f}|q = 0\rangle, \tag{4.27}$$

If $\vec{f}$ evolves according to the differential equation

$$\partial_t \vec{f} = \Omega(\vec{f}), \tag{4.30}$$

differentiating Eq. (4.28) with respect to time gives

$$\partial_t \left|\vec{f}(\vec{x},t)\right\rangle = -i\vec{\hat{p}} \cdot \Omega(\vec{f}(\vec{x},t)) \left|\vec{f}(\vec{x},t)\right\rangle. \tag{4.31}$$

We can bring it down to the Schrödinger form by defining the Hamiltonian

$$\hat{H} = \vec{\hat{p}} \cdot \Omega(\vec{f}(\vec{x},t)) = \vec{\hat{p}} \cdot \Omega(\vec{\hat{q}}), \tag{4.32}$$

METHODS

Quantum Machine Learning
(QML)

16

NYU

QUANTUM MACHINE LEARNING

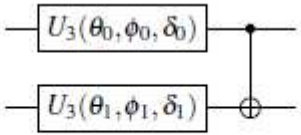

Figure 5.2: A quantum circuit showing the minimum viable entangling layer

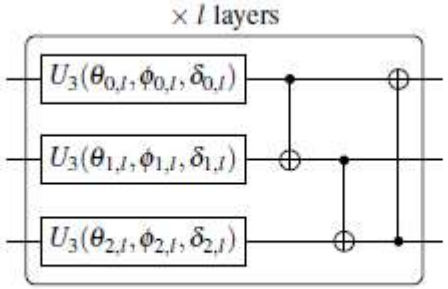

Figure 5.3: A quantum circuit showing an entangling layer with periodic CNOTs

CONTRIBUTIONS

CL of LBM

21

NYU

EXACT LINEARIZATION OF THE COLLISION OPERATOR

$$\vec{\Omega} = F_1 \vec{f}(1) + F_2 \vec{f}^{(2)} + \vec{F}_0$$

$$\vec{F}_0 = \frac{\Delta t}{\tau} \begin{pmatrix} \frac{1}{6} \\ \frac{2}{3} \\ \frac{1}{6} \end{pmatrix} \qquad (3.69)$$

where F_1 and F_2, for the D1Q3 are:

$$F_1 = -\frac{\Delta t}{\tau} \begin{pmatrix} \frac{1}{2} & 0 & \frac{1}{2} \\ 0 & 1 & 0 \\ \frac{1}{2} & 0 & \frac{1}{2} \end{pmatrix}$$

For the collision problem considered in linearizing the collision term classically, $\Delta x_i = 0$, such that one is able to verify:

$$\Sigma_j C_{ij}^{(1)(2)} E_j^{(2)}(\vec{x}, t) = 0 \qquad (3.82)$$

and:

$$F_2 = -\frac{\Delta t}{\tau} \begin{pmatrix} -\frac{1}{2} & -\frac{1}{2} & 1 \\ 1 & 1 & -2 \\ -\frac{1}{2} & -\frac{1}{2} & 1 \end{pmatrix}$$

$$\varepsilon_{max} = O(\Delta t \Delta x^{O_c}) \qquad (3.84)$$

NYU

LOGISTIC EQUATION

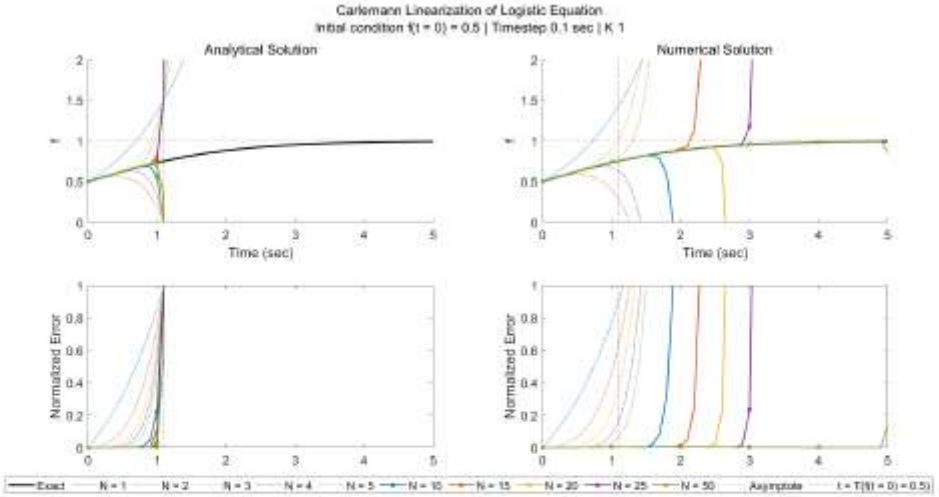

Figure 3.5: The analytical (left) (analytical integration) and numerical (right) (discrete time-stepping) solutions of the Carleman-linearized logistic equation are shown with their corresponding errors (bottom) as a function of time, varying initial conditions and Carleman linearization orders. The predicted time of validity is shown as a vertical asymptote in each plot.

NYU

D1Q3 COLLISION

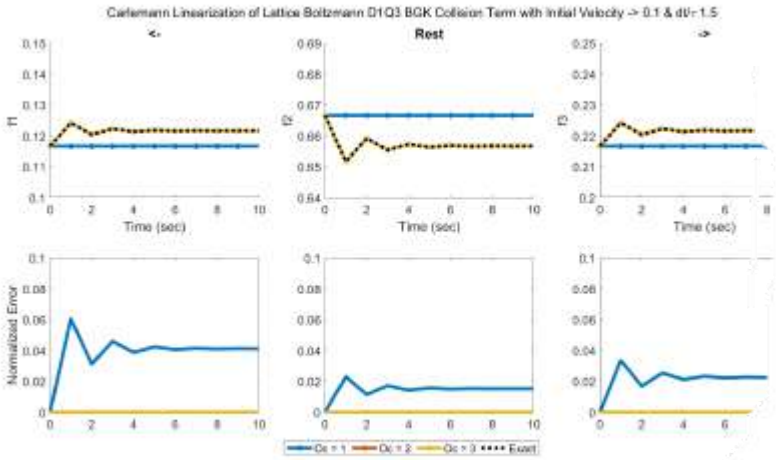

(d) $\frac{\Delta t}{\tau} = 1.5$

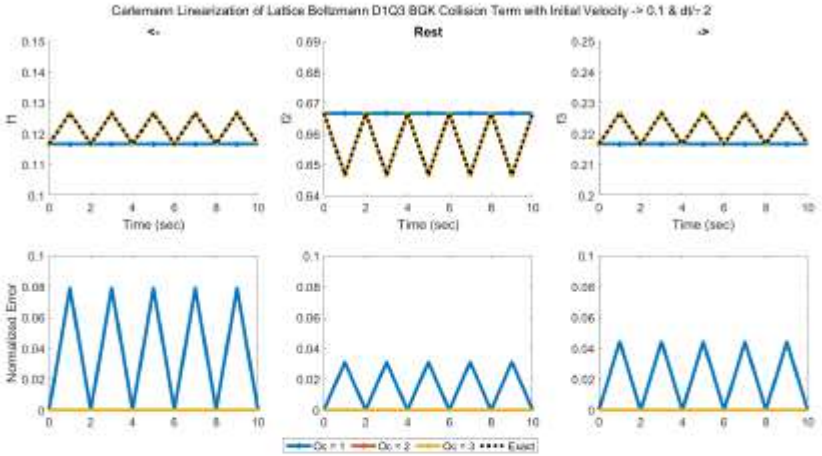

(f) $\frac{\Delta t}{\tau} = 2$

Figure 3.6: The solution of the discrete densities of the fluid in D1Q3 for successive collisions is shown for different $\frac{\Delta t}{\tau}$, for the exact and Carleman-linearized formulations as a function of time and Carleman linearization order. The bottom figures show the normalized errors for each discrete density. Note that the solution is exact beyond the first linearization order.

MATRIX STRUCTURE OF THE COLLISION OPERATOR

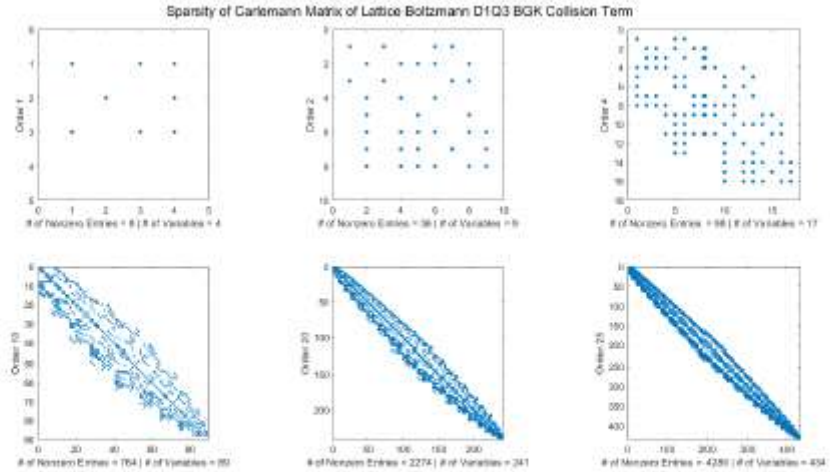

Figure 3.1: Visualization of the sparsity of the Carleman matrix for the collision term at various orders

NYU

CONTRIBUTIONS

CL of LBM (Caveat)

21

NYU

NONLINEARITY OF STREAMING

$$\frac{dV(\vec{x},t)}{dt} = \frac{\partial V(\vec{x},t)}{\partial t} + \vec{c}_i \cdot \Sigma_{i=1}^{Q} \frac{\partial V(\vec{x},t)}{\partial x_i} = CV \qquad (3.90)$$

$$\frac{\partial V_n(\vec{x},t)}{\partial f_j(\vec{x},t)} \frac{\partial f_j(\vec{x},t)}{\partial t} + \vec{c}_i \cdot \left(\frac{\partial V_n(\vec{x},t)}{\partial f_j(\vec{x},t)} \frac{\partial f_j(\vec{x},t)}{\partial x_i} \right) = C_n V \qquad (3.91)$$

CONCURRENT LINEARITY OF STREAMING & COLLISION

$$\rho = 1, \tag{3.93}$$

$$\partial_t \rho = 0. \tag{3.94}$$

$$\begin{aligned}\Sigma_{i,j=1}^{Q} \frac{dV_{ij}(\vec{x},t)}{dt} - \frac{\partial V_{ij}(\vec{x},t)}{\partial t} &= \Sigma_{i,j=1}^{Q} \vec{e}_i \cdot \nabla f_i f_j(\vec{x},t) + \vec{e}_j \cdot \nabla f_i f_j(\vec{x},t) - \vec{u} \cdot \nabla \rho - \vec{u} \cdot \nabla \rho \\ &= \Sigma_{i,j=1}^{Q} (\vec{e}_i + \vec{e}_j) \cdot \nabla f_i f_j(\vec{x},t).\end{aligned} \tag{3.100}$$

NYU

CONTRIBUTIONS

QLE for LBM & its Analysis

22

NYU

STREAMING OPERATOR

$$\vec{x} \rightarrow \vec{\hat{x}}$$
$$\hat{x}_d |\vec{x}\rangle = \frac{x_d}{N_d} |\vec{x}\rangle , \tag{4.83}$$

where N_d is the number of cells along the d^{th} dimension. There would be a corresponding momentum operator $\hat{v}_d$. Then, the streaming step, stemming from the advection term, for the $\vec{i}^{h}$ variable along the the d^{th} dimension could be implemented as

$$e^{-i\hat{v}_d \frac{c}{N_d} \hat{q}_i}. \tag{4.84}$$

HERMITICITY OF COLLISION HAMILTONIAN

Following [125], we first manipulate Eq. (4.32) to arrive at

$$\hat{H} = \frac{1}{2}\vec{\hat{p}}\cdot\Omega(\vec{\hat{q}}) + \frac{1}{2}\Omega(\vec{\hat{q}})\cdot\vec{\hat{p}} + (\frac{1}{2}\vec{\hat{p}}\cdot\Omega(\vec{\hat{q}}) - \frac{1}{2}\Omega(\vec{\hat{q}})\cdot\vec{\hat{p}}). \tag{4.38}$$

We can write the Hamiltonian as

$$\hat{H} = \frac{1}{2}\vec{\hat{p}}\cdot\Omega(\vec{\hat{q}}) + \frac{1}{2}\Omega(\vec{\hat{q}})\cdot\vec{\hat{p}} + \frac{1}{2}[\hat{p}_i, \Omega_i(\vec{\hat{q}})], \tag{4.39}$$

$$\Sigma_{i=1}^{Q}\frac{\partial}{\partial \hat{q}_i}\Omega_i(\hat{q}) = \Sigma_{i=1}^{Q}\frac{\partial}{\partial f_i}\Omega_i(\vec{f}) = -\frac{1}{\tau}(Q-D)$$

$$= \begin{cases} -\frac{2}{\tau}\hat{I} & D1Q3 \\ -\frac{7}{\tau}\hat{I} & D2Q9 \\ -\frac{24}{\tau}\hat{I} & D3Q27 \end{cases} \tag{4.42}$$

We define a normalized state

$$\left|\vec{f}'(\vec{x},t)\right\rangle = e^{\frac{1}{2}\int_0^t \nabla\cdot\vec{\Omega}(\vec{f})dr}\left|\vec{f}(\vec{x},t)\right\rangle.$$

$\left|\vec{f}'(\vec{x},t)\right\rangle$ evolves under the Hermitian Hamiltonian

$$\hat{H}' = \frac{1}{2}\Sigma_{i=1}^{Q}\hat{p}_i\Omega_i(\vec{\hat{q}}) + \Omega_i(\vec{\hat{q}})\hat{p}_i = \hat{H}'^{\dagger}.$$

NYU

GATE DECOMPOSITION OF BOSONIC HAMILTONIAN

$$\hat{q}_i = \frac{\sqrt{[N+1]}}{2}\Sigma_{j=0}^{q_c-1}\left(\sqrt{\frac{\hat{I}}{2^j}+\Sigma_{k=0}^{j-1}\left(\frac{\hat{n}_{k,i}}{2^k}\right)}\hat{X}_{j,i}\bigotimes_{k=j+1}^{q_c-1}(\hat{X}_{k,i})\right), \tag{4.95}$$

$$\hat{p}_i = \frac{\sqrt{[N+1]}}{2}\Sigma_{j=0}^{q_c-1}\left(\sqrt{\frac{\hat{I}}{2^j}+\Sigma_{k=0}^{j-1}\left(\frac{\hat{n}_{k,i}}{2^k}\right)}\hat{Y}_{j,i}\bigotimes_{k=j+1}^{q_c-1}(i\hat{Y}_{k,i})\right), \tag{4.96}$$

$$\hat{n} = \begin{pmatrix} 0 & 0 \\ 0 & 1 \end{pmatrix}, \tag{4.98}$$

$$\hat{n}_{k,i} = \frac{1}{2}(\hat{I}-\hat{Z}_{k,i}),$$

NYU

QUANTUM LINEAR EMBEDDING ERROR

$$\begin{aligned}\varepsilon(t+\Delta t) &\leq \Delta t\, Q\|A\|_\infty\left(\frac{1}{1-\varepsilon(t)-\varepsilon_N}+\frac{1}{1-(1-\varepsilon(t)-\varepsilon_N)^2}\right)\\ &= \Delta t\, Q\|A\|_\infty\left(\frac{1}{1-\varepsilon(t)-\varepsilon_N}+\frac{1}{1-(1-\varepsilon(t)-\varepsilon_N)^2}\right)\\ &= \Delta t\, Q\|A\|_\infty\left(\frac{(1-(1-\varepsilon(t)-\varepsilon_N)^2)+(1-\varepsilon(t)-\varepsilon_N)}{(1-\varepsilon(t)-\varepsilon_N)(1-(1-\varepsilon(t)-\varepsilon_N)^2)}\right)\\ &= \Delta t\, Q\|A\|_\infty\frac{3-\varepsilon(t)-\varepsilon_N}{(1-\varepsilon(t)-\varepsilon_N)(2-\varepsilon(t)-\varepsilon_N)}.\end{aligned} \tag{4.257}$$

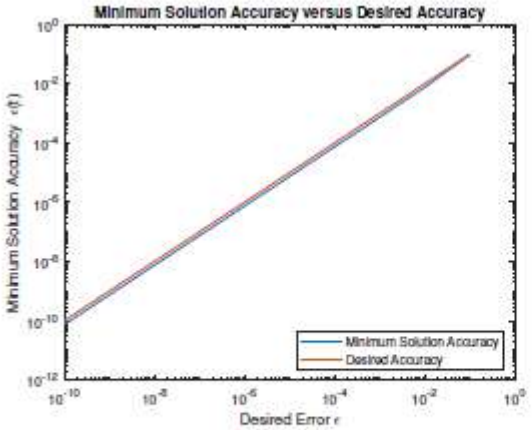

Figure 4.6: Minimum solution accuracy $\varepsilon(t)$ observed in time compared to the desired accuracy ε for $\Delta t\, Q\|A\|_\infty = \frac{1}{2}\varepsilon$

$$\Delta t\, Q\|A\|_\infty \leq \frac{1}{2}\varepsilon, \tag{4.258}$$

QUANTUM LINEAR EMBEDDING ERROR

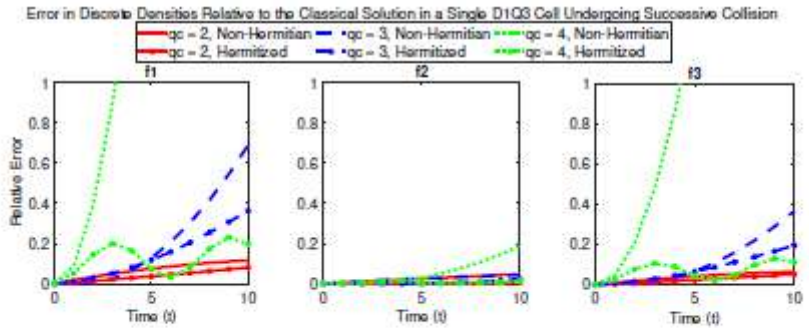

Figure 4.5: A comparison of the relative error the quantum solution for the discrete densities with respect to the classical solution using the non-Hermitian Hamiltonian (dashes) and the Hermitian Hamiltonian with post-processed dissipation (stars), for qubit counts (qc) of 2,3 and 4 for each variable.

QUANTUM LINEAR EMBEDDING COMPLEXITY

Table 4.5: Summary of the full algorithm (streaming and unitary collision) qubit and gate complexities with different streaming approaches. G is the lattice volume, D the number of dimensions, T total number of time steps taken, Q number of discrete densities, and N number of excitation levels/linearization order considered. ELP: Unitary Streaming by Embedding of Lattice Position SDDR: Unitary Streaming by Swapping Discrete Density Registers PCAM*: Streaming is performed classically after measurement of post-collision densities at each timestep

Streaming	Qubit Complexity (O)	LCU Ancillas (O)	Gate Complexity (O)
ELP	$\log_2(G)+Q(max(\log_2(G),\log_2(N+1)))$	$\log_2(QD\lceil\log_2(G)\rceil)$	$TQ^2D^2\lceil\log_2^2(G)\rceil+\frac{1}{\epsilon}Q^5T(N+1)^{\frac{5}{2}}\lceil\log_2(N$ $)\rceil^9$
SDDR	$min(G,T+\log_2(G))Q\log_2(N+1)$	$\log_2(Q\log_2(N+1))$	$\frac{1}{\epsilon}Q^5T(N+1)^{\frac{5}{2}}\lceil\log_2(N+1)\rceil^9+TQG$
PCAM*	$Q\log_2(N+1)+\log_2(G)+2D$	$\log_2(Q\log_2(N+1))$	$G\frac{1}{\epsilon}Q^5T(N+1)^{\frac{5}{2}}\lceil\log_2(N+1)\rceil^9$

QUANTUM LINEAR EMBEDDING COMPLEXITY

Table 4.6: Summary of the full algorithm (streaming and unitary collision) qubit and gate complexities with different streaming approaches in terms of the Reynolds number Re and the number of dimensions of the domain D. G is the lattice volume, D the number of dimensions, and ϵ the absolute difference error of the solution. ELP: Unitary Streaming by Embedding of Lattice Position SDDR: Unitary Streaming by Swapping Discrete Density Registers PCAM*: Streaming is performed classically after measurement of post-collision densities at each timestep

Streaming	Qubit Complexity (O)	LCU Ancillas (O)	Gate Complexity (O)
ELP	$\log_2(Re)+(max(\log_2(Re),\log_2\log\frac{1}{\epsilon}))3^D$	D	$Re^{\frac{3}{4}}\lceil\log_2^2(Re)\rceil 27^D D^2\frac{1}{\epsilon}+Re^{\frac{7}{4}}729^D\frac{1}{\epsilon}(\log_1 0\frac{1}{\epsilon})^{\frac{5}{2}}\lceil\log_2^9\log_1 0\frac{1}{\epsilon}\rceil$
SDDR	$min(Re^{\frac{9}{4}},Re^{\frac{3}{4}}3^D\frac{1}{\epsilon}+\log_2(Re))3^D\log_2\log_1 0\frac{1}{\epsilon}$	D	$Re^{\frac{7}{4}}729^D\frac{1}{\epsilon}(\log_1 0\frac{1}{\epsilon})^{\frac{5}{2}}\lceil\log_2^9\log_1 0\frac{1}{\epsilon}\rceil+Re^3\frac{1}{\epsilon}9^D$
PCAM*	$3^D\log_2\log_1 0\frac{1}{\epsilon}+\log_2(Re)+2D$	D	$Re^4 729^D\frac{1}{\epsilon}(\log_1 0\frac{1}{\epsilon})^{\frac{5}{2}}\lceil\log_2^9\log_1 0\frac{1}{\epsilon}\rceil$

CONTRIBUTIONS

QML for LBM Collision

23

NYU

BINARY VS. AMPLITUDE ENCODING

- **Binary**

$$|f_i\rangle = \Sigma_{n=0}^{2^b-1} \alpha_{n,i} |n\rangle = \Sigma_{n=0}^{2^b-1} \alpha_{n,i} \bigotimes_{s=0}^{b-1} |n_s\rangle, \tag{5.4}$$

where $n_s \in \{0,1\}$ is the s^{th} digit in the b-bit long binary string representing f_i. Moreover, the overall state is normalized such that

$$\Sigma_{n=0}^{2^b-1} |\alpha_{n,i}|^2 = 1. \tag{5.5}$$

$$|1100\rangle \qquad \frac{1}{2^1}1 + \frac{1}{2^2}1 + \frac{1}{2^3}0 + \frac{1}{2^4}0 = 0.5 + 0.25 = 0.75. \tag{5.3}$$

- **Modified Amplitude**

$$|\vec{y}\rangle = \frac{1}{\sqrt{N}} \Sigma_{i=0}^{N-1} |i\rangle \left(\sqrt{1-y_i^2}|0\rangle + y_i|1\rangle\right). \tag{5.8}$$

NYU

COMPATIBLITY WITH EXACT STREAMING

$$\frac{1}{\sqrt{Q}}\Sigma_{i=1}^{Q}|\vec{e}_i\rangle|f_i\rangle, \qquad (5.2)$$

Table 5.2: States encoding the different directions for a given dimension

Direction	$\|\vec{e}_i, d\rangle = \|e_{i,0}e_{i,1}\rangle$
Stationary	$\frac{1}{\sqrt{2}}(\|01\rangle + \|10\rangle)$
Positive Axis	$\|11\rangle$
Negative Axis	$\|00\rangle$

LOSS DEFINITION

$$\vec{x} = \vec{x}_{D2Q9} = \frac{1}{3}\begin{pmatrix} f_0 \\ \vdots \\ f_i \\ \vdots \\ f_8 \\ \rho \\ \|\vec{u}\| \end{pmatrix} \tag{5.11}$$

$$RMSE(\vec{x}) = \sqrt{\frac{1}{N}\Sigma_{n=1}^{N}(\Sigma_{\forall x_{i,n}\in\vec{x}_n}(\tilde{x}_{i,n} - x_{i,n})^2)}. \tag{5.10}$$

$$Loss = RMSE(\vec{x}). \tag{5.12}$$

HARD-WIRED SYMMETRIES FOR DATA AUGMENTATION

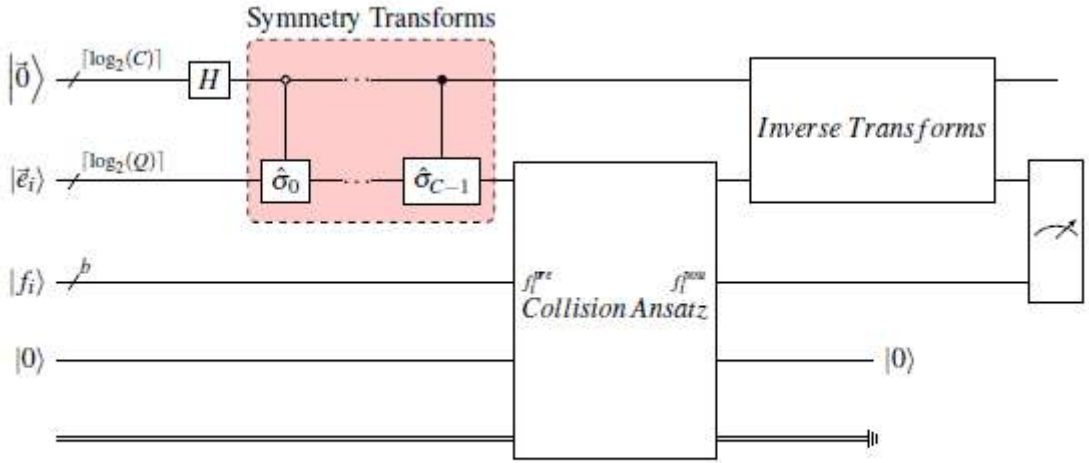

Figure 5.1: Overview of the quantum circuit used for training, including the lattice basis vector, value, and lattice site registers, as well as the ancilla qubits.

SYMMETRIES

- Scale Equivariance
- Rotation and reflection equivariance
- Mass and momentum invariance
- Positivity of discrete densities

$$\vec{f}^{post} = \frac{1}{8}\Sigma_{\hat{\sigma}\in D_8}\hat{\sigma}^{-1}\hat{N}\hat{\sigma}\vec{f}^{pre}, \quad (5.14)$$

$$D_8 = \hat{I}, \hat{r}, \hat{r}^2, \hat{r}^3, \hat{s}, \hat{r}\hat{s}, \hat{r}^2\hat{s}, \hat{r}^3\hat{s}, \quad (5.13)$$

Table 5.4: Cardinality (C) and qubit count for the rotation and reflection equivariance symmetry group in each D dimensional lattice

Lattice	C	# of Qubits
D1Q3	2	1
D2Q9	8	3
D3Q27	48	6

NYU

COLLISION ANSATZ

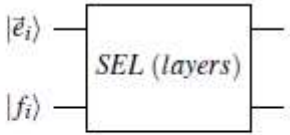

Figure 5.4: Quantum circuit of the strong collision ansatz

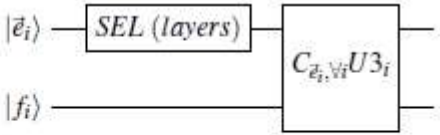

Figure 5.5: Quantum circuit of the strong-CU3 collision ansatz

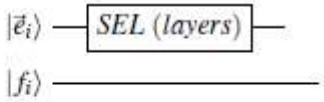

Figure 5.8: Quantum circuit of the Scramble collision ansatz

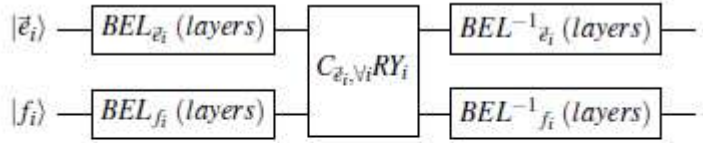

Figure 5.6: Quantum circuit of the BEL2-CRY-Inverse-BEL2 ansatz, an example of the EL(2)-COP-Inverse-EL(2) family of ansatz

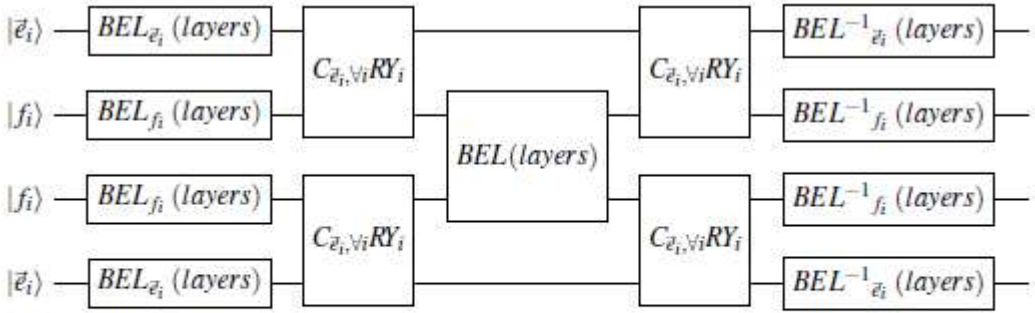

Figure 5.7: Quantum circuit of the BEL2-CRY-Inverse-BEL2 ansatz, an example of the EL(2)-COP-Inverse-EL(2) family of ansatz

COLLISION ANSATZ COMPLEXITY SCALING

Ansatz	1-Qubit Gate Count	2-Qubit Gate Count	Circuit Depth (<)	# of Parameters
BEL2-CRY-Inverse-BEL2	$2L(qc+b)$	$2L(qc+b)+2^{qc}bqc$	$2L(max(qc,b)+1)+2^{qc}bqc$	$L(qc+b)+2^{qc}b$
SEL2-CU3-Inverse-SEL2	$2L(qc+b)$	$2L(qc+b)+2^{qc}bqc$	$2L(max(qc,b)+1)+2^{qc}bqc$	$3(L(qc+b)+2^{qc}b)$
(SEL2-CU3)×R	$RL(qc+b)$	$R(L(qc+b)+2^{qc}bqc)$	$RL(max(qc,b)+1)+R2^{qc}bqc$	$3R(L(qc+b)+2^{qc}b)$
SEL-CRY-Inverse-SEL	$2Lqc$	$2Lqc+2^{qc}bqc$	$2L(qc+1)+2^{qc}bqc$	$3Lqc+2^{qc}b$
2^{nd} Order SEL-CRY-Inverse-SEL	$2Lbqc+4b^2$	$2Lbqc+2^{qc+1}bqc+2b^2$	$2L(qc+1)+2^{qc+1}bqc+2b+2b^2$	$3Lqc+2^{qc+1}b+12b^2$
Strong	L(qc+b)	L(qc+b)	L(qc+b+1)	3L(qc+b)

Table 5.3: Summary of key parameters of the major variations of the collision ansatz considered in this study, b corresponds to chosen binary precision, L, number of layers of the entangling layer as explained in Sec. 5.3.7.1, and qc number of qubits in the lattice index register $\lceil \log_2 Q \rceil$

EVOLUTION OF THE PURITY OF THE BINARY ENCODING

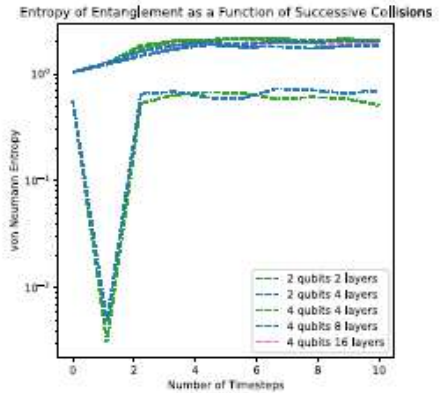

(a) Entropy of entanglement for a dataset of 32 samples for 10 consecutive collision steps

NYU

INCLUSION OF AN ANCILLA

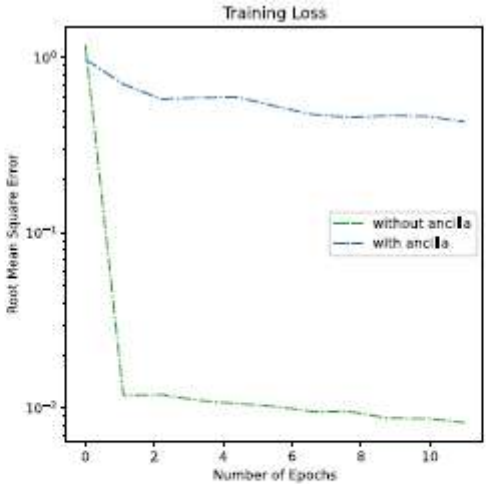

Figure 5.12: The 8-bit circuits with and without an ancilla are trained on a larger dataset of 100,000, after the initial training with 32 samples, for only 200 epochs. The circuits appear to reach loss values comparable to their optimal loss for the 32-sample weights within 10 epochs.

PHYSICS-INFORMED ANSATZ

# of Layers	Learning Rate	Batch Size	Sample Size	# of Epochs	Processed Count (rounded to nearest 10^6)	Loss
16	0.1	262,144	1,048,576	10	10	0.08318
				20	21	0.03704
				30	31	0.01331
	0.01	262,144	1,048,576	40	42	0.6407
				50	52	0.08484
	0.001	262,144	1,048,576	60	63	0.3085
				70	73	0.04147
				80	84	0.001032
				100	105	0.000565
20	0.1	262,144	1,048,576	10	10	0.0073727
	0.01	262,144	1,048,576	10	10	0.002292
				15	16	0.04326
	0.001	262,144	1,048,576	15	16	0.006037
				20	21	0.008651
				30	31	0.004102
	0.0001	262,144	1,048,576	40	42	0.008136

Table 5.10: Parameters and loss of the training of SEL-CRY-Inverse-SEL collision ansatz with amplitude encoding

NYU

PHYSICS-INFORMED ANSATZ WITH SYMMETRIES

# of Layers	Learning Rate	Batch Size	Sample Size	# of Epochs	Processed Count (rounded to nearest 10^6)	Loss
64	0.1	262,144	1,048,576	10	10	0.03933
				20	21	0.005144
				30	31	0.001867
				40	42	0.004426
				50	52	0.004056
				60	63	0.001527
	0.01	262,144	1,048,576	70	73	0.001962
				80	84	0.002453
				90	94	0.00472
				100	105	0.001967
				200	210	0.000396

Table 5.12: Parameters and loss of the training of SEL-CRY-Inverse-SEL collision ansatz with amplitude encoding and symmetry transforms

GENERAL (STRONG) ANSATZ

# of Layers	Learning Rate	Batch Size	Sample Size	# of Epochs	Processed Count (rounded to nearest 10^6)	Loss
8	0.1	262,144	1,048,576	10	10	0.02103
				20	21	0.00189
				30	31	0.00185
				40	42	0.00213
				50	52	0.00101
64	0.1	262,144	1,048,576	10	10	0.03223
				20	21	0.00353
				30	31	0.00169
				40	42	0.00293
				50	52	0.00178
				60	63	0.00132
	0.01	262,144	1,048,576	70	73	0.00152
				80	84	0.00156
				90	94	0.00201
				100	105	0.00374

Table 5.13: Parameters and loss of the training of Strong collision ansatz with amplitude encoding and symmetry transforms

NYU

ERROR PROPAGATION

$$\sigma_{f_i}^2(t) = B\frac{1-A^t}{1-A}\forall t \geq 0, \tag{5.36}$$

$$A = (1-\frac{\Delta t}{\tau})^2 + Q(\frac{\Delta t}{\tau})^2((\partial_\rho f_i^{eq})^2 + 2(\partial_{\|u\|} f_i^{eq})^2) \tag{5.37}$$

$$B = (\frac{\Delta t}{\tau})^2((\partial_\rho f_i^{eq})^2 b_1^2 + 2(\partial_{\|u\|} f_i^{eq})^2 b_2^2). \tag{5.38}$$

RMSE obtained, (3.69×10^{-4}) $Re = O(10)$

RSME of $O(10^{-6})$ to $T_{max} = O(10^6)$ or $Re = O(10^5)$.

ERROR RATIO OF THE POST-COLLISION VELOCITIES

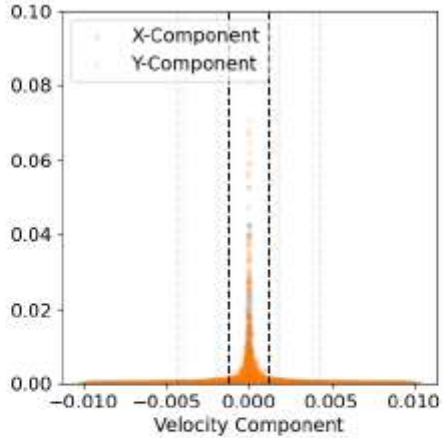

Figure 5.13: The post-collision error ratio of the x-(blue) and y-(orange) velocity components is shown against the value of the respective component. The vertical dashed lines in blue, orange and grey represent the x-, y-component and combined standard deviation of the error distribution. The black vertical dashed line represents the unscaled training loss.

DEMONSTRATION WITH LID-DRIVEN CAVITY

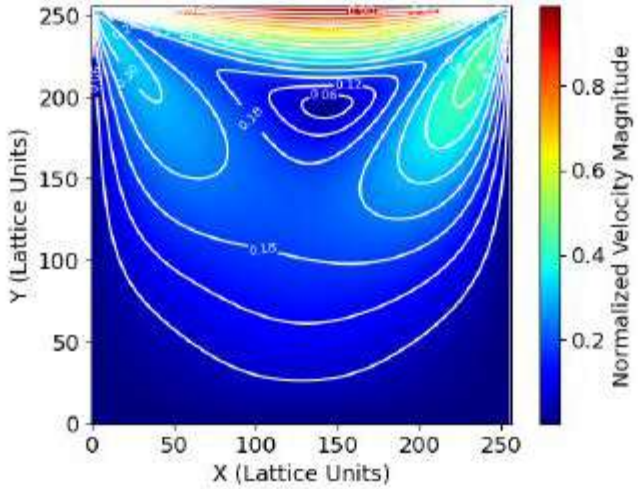

Figure 5.14: Normalized velocity magnitude corresponding to the flow field of the lid-driven cavity solved using the lattice Boltzmann method with the standard classical BGK collision at Re = 40 on a 256 × 256 grid; The whit contours represent the isovelocity lines

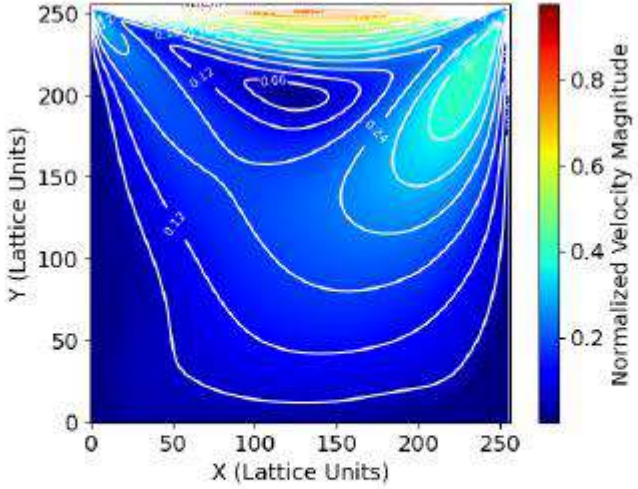

Figure 5.15: Normalized velocity magnitude corresponding to the flow field of the lid-driven cavity solved using the lattice Boltzmann method with the quantum collision at Re = 40 on a 256 × 256 grid; The white contours represent the isovelocity lines

EPILOGUE

Summary of Key Contributions

30

NYU

SUMMARY

- Physically justifying the Carleman linearization of lattice Boltzmann
- Exactly linearizing the collision term and showing the convergence of error when streaming is considered
- Mapping the quantum linear embedding method to digital quantum computers
- Developing the complexity and error analysis of quantum linear embedding in a finite Hilbert space
- Determining conditions of convergence of truncated linear embedding error for an arbitrary polynomial
- Developing the first quantum algorithm for lattice Boltzmann with unitary collision and streaming
- Performing the first regression task in quantum machine learning with a binary encoding
- Using quantum machine learning to train a collision operator compatible with exact streaming
- Demonstrating that the linearization error and instabilities arise from the smallest velocities considered

EPILOGUE

Acknowledgements

32

NYU

THANK YOU!

NYU